

Fluctuations of Power versus Energy for Random Fields Near a Perfectly Conducting Boundary

Luk R. Arnaut

Abstract—The standard deviations of the energy and Poynting power densities for an isotropic random field near a perfectly conducting planar boundary are characterized, based on quartic plane-wave expansions. For normal and transverse components, different rates of decay exist as a function of electrical distance from the boundary. At large distances, the envelopes for the power are more strongly damped than for the energy, both showing inverse power law decay. The decay for the standard deviation is generally one order faster than for the corresponding mean. For the normally directed power flux, its standard deviation near the boundary increases linearly with distance. The relative uncertainty of the scalar power is much smaller than for the Poynting power. Poynting’s theorem for standard deviations is obtained and demonstrates larger standard deviations of the energy imbalance and power flux than their mean values.

Index Terms—Boundary zone fields, complex cavity, energy, measurement, noise, power, standard deviation.

I. INTRODUCTION

THE characterization of the fluctuations of complex random fields, energy, and power near an electromagnetic (EM) boundary is an aspect of fundamental importance. Some recent studies include the evaluation of linear and orbital angular momentum near a ground plane [1], the probing of fields near a metal wall in a mode-stirred reverberation chamber (MSRC) [2], and the propagation of uncertainty and correlation in computational EM field solvers [3].

When measuring deterministic fields, practitioners have a choice between electric (or magnetic) field sensors of wire dipole (or loop) type versus aperture antennas or waveguides that measure EM power flow. The choice is largely governed by the sensitivity at the frequency of interest, the size and practicality. For plane waves, the conversion from voltage, field intensity, electric (or magnetic) energy to EM power is straightforward.

Random fields near an EM boundary prompt a consideration of the effects of the boundary conditions on the root-mean-square (RMS) fluctuations (standard deviation) of power vs. energy. Any such effects complement those that have been found to exist for their expected values (averages) [1], which governs the optimal sensor placement for eliminating the effect of the boundary. As will be shown here, the choice of sensor type and measurand leads to supplementary differences in the signal-to-noise ratio (SNR) between random energy vs. random power that affect their relative uncertainties.

In [4], the issue of defining power in an ideal reverberant space was raised. While the *average* local power is null across all angles of incidence (4π sr), this does not preclude significant nonzero fluctuations of power that may still produce physical effects and require characterization. Near a perfect

electric conducting (PEC) boundary, the average power [1] and energy [5]–[8] of random fields are both nonzero and exhibit different spatial dependencies, through decaying interference at-a-distance, unlike for deterministic fields. One consequence is the recommendation to avoid using a boundary layer zone of quarter-wavelength thickness near any metallic surface inside a MSRC [9]. However, this guard distance creates practical problems in testing heavy floor-standing equipment or inside small cabinets. More generally, it is wasteful of the available interior space, particularly at relatively low frequencies. Some studies have started to address this issue [1, sec. III-C], [10], [11, sec. 5.3.5], [12], with a view to increase the working volume of a MSRC up to its physical boundaries. To this end, the full statistical characterization of the EM energy and power in the boundary zone is required.

In this article, the work in [1], [5], [6], [10] on average energy and Poynting power densities for random fields near a PEC boundary is extended to cover corresponding standard deviations. A time-harmonic dependence $\exp(j\omega t)$ is assumed and suppressed. To simplify notation, the argument of all spherical Bessel functions will be dropped, i.e., $j_\ell \equiv j_\ell(2kz)$ for $\ell = 0, 1, 2$, which are hence always evaluated at $2kz$.

II. SPECTRAL PLANE WAVE EXPANSIONS FOR QUARTIC MIXED PRODUCTS OF CIRCULAR GAUSSIAN FIELDS

The angular spectral plane-wave expansion is defined by

$$\underline{F}(\underline{r}) = \frac{1}{\Omega} \iint_{\Omega} \underline{\mathcal{F}}(\Omega) \exp(-j\mathbf{k} \cdot \underline{r}) d\Omega \quad (1)$$

where $\underline{F} = \underline{E}$ or \underline{H} and $\underline{\mathcal{F}} = \underline{\mathcal{E}}$ or $\underline{\mathcal{H}}$, which can be traced to Cramér’s spectral representation of scalar stationary random functions [5], [13]. For the time-averaged local electric and magnetic energy densities, $U_e(\underline{r}) = \epsilon_0 \underline{E}(\underline{r}) \cdot \underline{E}^*(\underline{r})/4$ and $U_m(\underline{r}) = \mu_0 \underline{H}(\underline{r}) \cdot \underline{H}^*(\underline{r})/4$, and for the Poynting power vector $\underline{S}(\underline{r}) = [\underline{E}(\underline{r}) \times \underline{H}^*(\underline{r})]/2$, the expansions involve two-factor pure or mixed products of plane wave fields, viz., [1]

$$F_\alpha(\underline{r}) G_\beta^*(\underline{r}) = \frac{1}{\Omega} \left(\iint_{\Omega} \right)^2 \mathcal{F}_{1,\alpha} \mathcal{G}_{2,\beta}^* \delta(\Omega_{12}) \times \exp[-j(\underline{k}_1 - \underline{k}_2^*) \cdot \underline{r}] d\Omega_1 d\Omega_2 \quad (2)$$

for $F, G \in \{E, H\}$; $\mathcal{F}, \mathcal{G} \in \{\mathcal{E}, \mathcal{H}\}$; $\alpha, \beta \in \{x, y, z\}$, and where $\mathcal{F}_{i,\alpha} \triangleq \underline{\mathcal{F}}(\Omega_i) \cdot \underline{1}_\alpha$, etc., are Cartesian field components along the direction of $\underline{1}_\alpha$ for the angular spectral plane-wave components ($\underline{\mathcal{E}}(\Omega_i), \underline{\mathcal{H}}(\Omega_i), \underline{k}_i$) of the observable random EM field ($\underline{E}, \underline{H}$) at location of incidence \underline{r} . The wave vector $\underline{k}_i \triangleq \underline{k}(\Omega_i)$ is quasi-monochromatic ($|\underline{k}_i| = \omega_i \sqrt{\mu_0 \epsilon_0}$). The analysis assumes a lossless medium of incidence ($\mathcal{E}_i/\mathcal{H}_i = \mathcal{E}_0/\mathcal{H}_0 = \eta_0 = \sqrt{\mu_0/\epsilon_0}$; $\underline{k}_i = \underline{k}_i^*$). The symmetric set difference $\Omega_{ij} \triangleq$

$\Omega_i \Delta \Omega_j = (\Omega_i \cup \Omega_j) \setminus (\Omega_i \cap \Omega_j)$ for overlap between solid angles Ω_i and Ω_j satisfies $\delta(\Omega_{ij} = \emptyset) = 1$ and $\delta(\Omega_{ij} \neq \emptyset) = 0$. The differentials $d\Omega_i = \sin \theta_i d\theta_i d\phi_i$ refer to standard spherical angles of azimuth ϕ_i and elevation θ_i , measured from zenith, for integration across the upper hemisphere $\Omega = 2\pi$ sr ($z \geq 0$).

The second-order expansions (2) suffice for the calculation of ensemble averages (expected values) of energy and power, denoted by $\langle \cdot \rangle$. Using a TE/TM decomposition and enforcing the EM boundary conditions at the PEC plane oxy [1], [5]

$$\langle S_\alpha(kz) \rangle = \langle S_t(kz) \rangle = 0, \quad \alpha = x, y \quad (3)$$

$$\langle S_z(kz) \rangle = \langle S(kz) \rangle = -j \frac{\langle |\mathcal{E}_0|^2 \rangle}{\eta_0} j_1 \quad (4)$$

$$\langle U_\alpha(kz) \rangle = \frac{\varphi_0 \langle |\mathcal{F}_0|^2 \rangle}{3} \left(1 \mp j_0 \pm \frac{j_2}{2} \right), \quad \alpha = x, y \quad (5)$$

$$\langle U_z(kz) \rangle = \frac{\varphi_0 \langle |\mathcal{F}_0|^2 \rangle}{3} (1 \pm j_0 \pm j_2) \quad (6)$$

$$\langle U_t(kz) \rangle = \frac{2\varphi_0 \langle |\mathcal{F}_0|^2 \rangle}{3} \left(1 \mp j_0 \pm \frac{j_2}{2} \right) \quad (7)$$

$$\langle U(kz) \rangle = \varphi_0 \langle |\mathcal{F}_0|^2 \rangle \left(1 \mp \frac{j_0}{3} \pm \frac{2j_2}{3} \right) \quad (8)$$

where upper and lower signs correspond to electric ($U = U_e$) and magnetic ($U = U_m$) energy densities, respectively, and $\varphi_0 \langle |\mathcal{F}_0|^2 \rangle \triangleq \epsilon_0 \langle |\mathcal{E}_0|^2 \rangle = \mu_0 \langle |\mathcal{H}_0|^2 \rangle$. The subscripts α, z , and t represent 1-D tangential, 1-D normal, and 2-D tangential (xy -) components, respectively. Absence of a subscript refers to the 3-D full (vector) field \underline{E} or \underline{H} . The total (combined, summed) electric and magnetic energy will be denoted as U_{em} .

The expectations (3)–(8) presume a set of orthogonality conditions to hold for the second-order moments of the local plane-wave complex fields $\mathcal{F}_i \equiv \mathcal{F}'_i - j\mathcal{F}''_i = \mathcal{F}_{i,\phi} \underline{1}_{\phi_i} + \mathcal{F}_{i,\theta} \underline{1}_{\theta_i}$ in the transverse plane $o\phi_i\theta_i$, viz., [4], [13]

$$C_{\mathcal{F}'_{i,\phi} \mathcal{F}'_{j,\phi}} = C_{\mathcal{F}'_{i,\theta} \mathcal{F}'_{j,\theta}} = (\langle |\mathcal{E}_0|^2 \rangle / 4) \delta(\Omega_{ij}) \quad (9)$$

for the in-phase/in-phase (I/I) and quadrature/quadrature (Q/Q) covariances $C_{\mathcal{F}'_{i,\cdot} \mathcal{F}'_{j,\cdot}} = \langle \mathcal{F}'_{i,\cdot} \mathcal{F}'_{j,\cdot} \rangle$. The delta correlation in (9) is a consequence of the assumed stationarity (i.e., statistical homogeneity and isotropy) of incident \underline{E} with respect to \underline{r} . For the I/Q and cross-component covariances, the conditions are

$$C_{\mathcal{F}'_{i,\phi} \mathcal{F}''_{j,\phi}} = C_{\mathcal{F}'_{i,\theta} \mathcal{F}''_{j,\theta}} = C_{\mathcal{F}'_{i,\phi} \mathcal{F}'_{j,\theta}} = 0. \quad (10)$$

The expansion (2) can be extended to quartic forms, as required in the calculation of second-order moments of U_e , U_m , U_{em} and S involving pure or pairwise mixed fourth-order moments of the fields, in the general form

$$F_\alpha(\underline{r}) F_\beta^*(\underline{r}) G_\gamma(\underline{r}) G_\delta^*(\underline{r}) = \frac{1}{\Omega} \left(\iint \int \int_{\Omega} \mathcal{F}_{1,\alpha} \mathcal{F}_{2,\beta}^* \mathcal{G}_{3,\gamma} \mathcal{G}_{4,\delta}^* \right. \\ \left. \times \exp[-j(\underline{k}_1 - \underline{k}_2^* + \underline{k}_3 - \underline{k}_4^*) \cdot \underline{r}] \delta(\Omega_{1234}) d\Omega_1 d\Omega_2 d\Omega_3 d\Omega_4 \right) \quad (11)$$

for any selection of pairwise conjugate orthogonal field components along $\alpha, \beta, \gamma, \delta \in \{x, y, z\}$, with $\delta(\Omega_{1234}) \equiv \delta(\Omega_1 \Delta \Omega_2 \Delta \Omega_3 \Delta \Omega_4) = \delta(\Omega_{12}) \delta(\Omega_{34})$. Now, if all \mathcal{F}_i and \mathcal{G}_j are taken to be *centered circular Gaussian* fields, then

$\langle \mathcal{F}_{1,\alpha} \mathcal{F}_{2,\beta}^* \mathcal{G}_{3,\gamma} \mathcal{G}_{4,\delta}^* \rangle$ can be expressed in terms of second-order moments only, without imposing additional fourth-order moment conditions, by applying Isserlis's theorem for Gaussian moments to the individual real and imaginary parts of $\mathcal{F}_{i,\alpha}$ and $\mathcal{G}_{j,\gamma}$. Expressing the kernel of (11) as a sum of products of pairwise covariances for real variates, followed by a recombination to the sought covariances of the complex fields, Isserlis's theorem for the complex plane-wave field components follows as

$$\langle \mathcal{F}_{1,\alpha} \mathcal{F}_{2,\beta}^* \mathcal{G}_{3,\gamma} \mathcal{G}_{4,\delta}^* \rangle = \langle \mathcal{F}_{1,\alpha} \mathcal{F}_{2,\beta}^* \rangle \langle \mathcal{G}_{3,\gamma} \mathcal{G}_{4,\delta}^* \rangle \\ + \langle \mathcal{F}_{1,\alpha} \mathcal{G}_{3,\gamma} \rangle \langle \mathcal{F}_{2,\beta}^* \mathcal{G}_{4,\delta}^* \rangle + \langle \mathcal{F}_{1,\alpha} \mathcal{G}_{4,\delta}^* \rangle \langle \mathcal{F}_{2,\beta}^* \mathcal{G}_{3,\gamma} \rangle. \quad (12)$$

For the mixed fourth moment $\langle |\mathcal{F}_{i,\alpha}|^2 |\mathcal{G}_{j,\gamma}|^2 \rangle$, its terms in (12) contain $\langle \mathcal{F}_{i,\alpha} \mathcal{G}_{j,\gamma} \rangle$ and $\langle \mathcal{F}_{i,\alpha} \mathcal{G}_{j,\gamma}^* \rangle$, which may vanish or not [1], as will become apparent in the further analysis.

In summary, the conditions (9) and (10) on the second-order moments are necessary and sufficient to fully characterize all even-order moments of circular complex Gaussian $\mathcal{F}_{i,\alpha}$ and $\mathcal{G}_{j,\gamma}$ and hence all (even and odd) moments of energy and power, following (12). If some fields are elliptic and/or non-Gaussian, then additional conditions on their pseudovariances and/or fourth-order moments apply, respectively.

Note that Isserlis's theorem can equally be applied to $\langle \mathcal{F}_{1,\alpha} \mathcal{F}_{2,\beta}^* \mathcal{G}_{3,\gamma} \mathcal{G}_{4,\delta}^* \rangle$, i.e., just as well to the actual (i.e., physical) fields F and G as to their spectral plane-wave source fields \mathcal{F} and \mathcal{G} , because of linearity for the superposition of Gaussian fields. For non-Gaussian \mathcal{F} and \mathcal{G} , however, (12) does not necessarily extend to moments of F and/or G .

III. POWER

A. 1-D Cartesian Tangential or Normal Power Flow

The complex Poynting vector \underline{S} has Cartesian components $S_\alpha \underline{1}_\alpha = [(E_\beta H_\gamma^* - E_\gamma H_\beta^*)/2] \underline{1}_\alpha$ where (α, β, γ) is a cyclic permutation of x, y and z . Their second-order moments are

$$\langle |S_\alpha|^2 \rangle = \frac{1}{4} (\langle |E_\beta|^2 |H_\gamma|^2 \rangle + \langle |E_\gamma|^2 |H_\beta|^2 \rangle \\ - \langle E_\beta H_\gamma^* E_\gamma H_\beta \rangle - \langle E_\beta^* H_\gamma E_\gamma H_\beta^* \rangle) \quad (13)$$

and are evaluated using (12) for $\mathcal{F} = \mathcal{E}$ and $\mathcal{G} = \mathcal{H}$, as follows.

First, for a 1-D component of the power flowing parallel to the boundary, i.e., tangential S_α with $\alpha = x$ or y , Isserlis's theorem for complex E_β, E_z, H_β and H_z leads to

$$\langle E_\beta H_z^* E_z H_\beta \rangle = \langle E_\beta^* H_z E_z H_\beta^* \rangle = 0 \quad (14)$$

with $\beta = y$ or x , respectively ($\beta \neq \alpha$), because $\langle E_\beta H_z^* \rangle = \langle E_\beta E_z^* \rangle = \langle E_\beta H_\beta \rangle = 0$, as follows from (2) [1]. The first two terms in (13) with $\langle E_\beta H_z^* \rangle = \langle E_z H_\beta^* \rangle = 0$ are

$$\left\{ \begin{array}{l} \langle |E_\beta(kz)|^2 |H_z(kz)|^2 \rangle \\ \langle |E_z(kz)|^2 |H_\beta(kz)|^2 \rangle \end{array} \right\} = \frac{4 \langle |\mathcal{E}_0|^2 \rangle^2}{9 \eta_0^2} \left(1 \mp 2j_0 \mp \frac{j_2}{2} \right. \\ \left. + j_0^2 - \frac{j_2^2}{2} + \frac{j_0 j_2}{2} \right) \quad (15)$$

where upper and lower signs refer to $\langle |E_\beta|^2 |H_z|^2 \rangle$ and $\langle |E_z|^2 |H_\beta|^2 \rangle$. Substituting (14) and (15) into (13) yields

$$\langle |S_\alpha(kz)|^2 \rangle = \frac{2 \langle |\mathcal{E}_0|^2 \rangle^2}{9 \eta_0^2} \left(1 + j_0^2 - \frac{j_2^2}{2} + \frac{j_0 j_2}{2} \right). \quad (16)$$

Combining (16) with $\langle S_\alpha \rangle = 0$ results in the standard deviation $\sigma_{S_\alpha} = \sqrt{\langle |S_\alpha|^2 \rangle - \langle S_\alpha \rangle^2}$ as

$$\sigma_{S_\alpha}(kz) = \sigma_{S_\alpha, \infty} \sqrt{1 + j_0^2 - \frac{j_2^2}{2} + \frac{j_0 j_2}{2}}, \quad \alpha = x, y \quad (17)$$

where its asymptotic value for $kz \rightarrow +\infty$ is

$$\sigma_{S_\alpha, \infty} = \frac{\sqrt{2} \langle |\mathcal{E}_0|^2 \rangle}{3\eta_0}. \quad (18)$$

Second, for the normally directed power flow S_z , we have

$$\langle E_x H_y^* E_y^* H_x \rangle = \langle E_x^* H_y E_y H_x^* \rangle = -\frac{\langle |\mathcal{E}_0|^2 \rangle^2}{\eta_0^2} j_1^2 \quad (19)$$

on account of $\langle E_x H_y^* \rangle = -\langle E_y^* H_x \rangle = -j \langle |\mathcal{E}_0|^2 \rangle j_1 / \eta_0$ and $\langle E_x E_y^* \rangle = 0 = \langle E_x H_x \rangle$, the other terms in (13) being

$$\begin{aligned} \langle |E_x(kz)|^2 |H_y(kz)|^2 \rangle &= \langle |E_y(kz)|^2 |H_x(kz)|^2 \rangle = \\ &= \frac{4 \langle |\mathcal{E}_0|^2 \rangle^2}{9\eta_0^2} \left(1 - j_0^2 + \frac{9j_1^2}{4} - \frac{j_2^2}{4} + j_0 j_2 \right) + \frac{\langle |\mathcal{E}_0^2 \rangle|^2}{\eta_0^2} j_1^2. \end{aligned} \quad (20)$$

In order to arrive at (20), the pseudocovariances $\langle E_x H_y \rangle = -\langle E_y H_x \rangle = -j \langle \mathcal{E}_0^2 \rangle j_1 / \eta_0$ were employed. However, $\langle \mathcal{E}_0^2 \rangle = 0$ owing to the assumed complex circularity of the plane-wave fields, whence the second term in (20) vanishes.¹ Hence, substituting (19) and (20) into (13) for $\alpha = z$ yields

$$\langle |S_z(kz)|^2 \rangle = \frac{2 \langle |\mathcal{E}_0|^2 \rangle^2}{9\eta_0^2} \left(1 - j_0^2 + \frac{9j_1^2}{2} - \frac{j_2^2}{4} + j_0 j_2 \right) \quad (21)$$

which, combined with the mean (4), results in

$$\sigma_{S_z}(kz) = \sigma_{S_z, \infty} \sqrt{1 - j_0^2 - \frac{j_2^2}{4} + j_0 j_2} \quad (22)$$

where

$$\sigma_{S_z, \infty} = \frac{\sqrt{2} \langle |\mathcal{E}_0|^2 \rangle}{3\eta_0}. \quad (23)$$

In Fig. 1(a), the standard deviations (17) and (22) are compared with numerical results obtained via Monte Carlo (MC) simulation of random plane waves, based on 30 random values of $|\mathcal{E}_0|$, 32 elevation angles, 16 azimuthal angles, and 16 polarization angles, evaluated at 362 logarithmically spaced distances kz ranging from 0.05 to 50. The value of σ_{S_x} reaches its maximum on the PEC surface, where σ_{S_z} vanishes. Local maxima and minima of $\sigma_{S_x}(kz)$ are found at distances that are marginally shorter than those for $\sigma_{S_z}(kz)$. The oscillations of $\sigma_{S_z}(kz)$ are more strongly damped than those for $\langle S_z(kz) \rangle$ [1, Fig. 1], as will be confirmed in sec. V by comparing their envelopes. For $kz \rightarrow +\infty$, it is verified that (17) and (22) merge, as expected for ideal isotropic fields in the absence of an EM boundary.

¹In the evaluation of $\langle |E_x(kz)|^2 |H_y(kz)|^2 \rangle$, particularly for relatively small data sets and in case of (residual) noncircularity, a small value of the pseudovariance $\langle \mathcal{E}_0^2 \rangle$ may still have a significant effect when $\langle |E_x(kz)|^2 |H_y(kz)|^2 \rangle$ is also small, particularly when $kz \ll 1$.

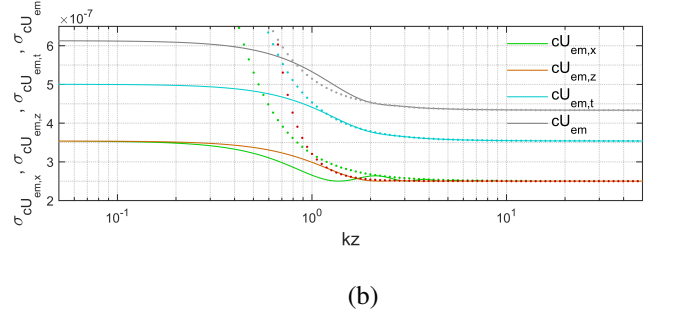
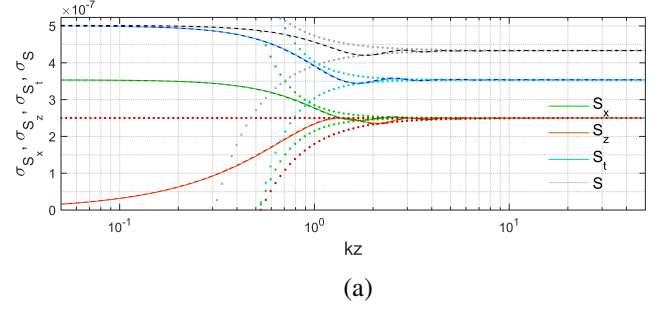


Fig. 1: Standard deviations, in units W/m^2 , based on $\langle \mathcal{E}_0'^2 \rangle^{1/2} = \langle \mathcal{E}_0''^2 \rangle^{1/2} = 0.01$ V/m, for (a) Poynting power $\sigma_{S_x}(kz)$, $\sigma_{S_z}(kz)$, $\sigma_{S_t}(kz)$, and $\sigma_S(kz)$ with upper and lower asymptotic envelopes $\Upsilon_{S(\alpha)}^\pm(kz \gg 3/2)$. Solid: theory; dashed: MC simulation; dotted: envelopes. Olive/green: S_x ; maroon/red: S_z ; blue/cyan: S_t ; black/gray: S ; and for (b) scalar power $\sigma_{cU_{em,x}}(kz)$, $\sigma_{cU_{em,z}}(kz)$, $\sigma_{cU_{em,t}}(kz)$, and $\sigma_{cU_{em}}(kz)$ with upper asymptotic envelopes $\Upsilon_{cU_{em,\alpha}}^+(kz \gg 3/2)$, shown using the same color scheme as in (a).

B. 2-D Tangential Power Flow

For the 2-D tangential Poynting vector $\underline{S}_t = S_x \underline{1}_x + S_y \underline{1}_y$, it follows that $|S_t|^2 \equiv \underline{S}_t^\dagger \cdot \underline{S}_t = |S_x|^2 + |S_y|^2$. With (12) and (3), this yields $\sigma_{S_t} = \sqrt{2} \sigma_{S_x}$ as

$$\sigma_{S_t}(kz) = \sigma_{S_t, \infty} \sqrt{1 + j_0^2 - \frac{j_2^2}{2} + \frac{j_0 j_2}{2}} \quad (24)$$

where

$$\sigma_{S_t, \infty} = \frac{2 \langle |\mathcal{E}_0|^2 \rangle}{3\eta_0}. \quad (25)$$

C. 3-D Spatial Power Flow

For the full Poynting vector $\underline{S} = \sum_{\alpha=x,y,z} S_\alpha \underline{1}_\alpha$, we have $|S|^2 \equiv \underline{S}^\dagger \cdot \underline{S} = |S_t|^2 + |S_z|^2$. With (12), (16) and (21),

$$\langle |S(kz)|^2 \rangle = \frac{2 \langle |\mathcal{E}_0|^2 \rangle^2}{3\eta_0^2} \left(1 + \frac{j_0^2}{3} + \frac{3j_1^2}{2} - \frac{5j_2^2}{12} + \frac{2j_0 j_2}{3} \right) \quad (26)$$

which, combined with (4), yields

$$\sigma_S(kz) = \sigma_{S, \infty} \sqrt{1 + \frac{j_0^2}{3} - \frac{5j_2^2}{12} + \frac{2j_0 j_2}{3}} \quad (27)$$

where

$$\sigma_{S, \infty} = \sqrt{\frac{2}{3}} \frac{\langle |\mathcal{E}_0|^2 \rangle}{\eta_0}. \quad (28)$$

IV. ENERGY

The standard deviations of $U_{e(\alpha)}$ and $U_{m(\alpha)}$ for circular Gaussian fields near an impedance boundary were derived in [8], [10], enabling all moments to be obtained merely by a single variate transformation.

For $|F_\alpha|^2$, setting $\mathcal{F}_\alpha = \mathcal{F}_\beta = \mathcal{G}_\gamma = \mathcal{G}_\delta$ in (12) and using $\langle \mathcal{F}_\alpha^2 \rangle = 0$ owing to the complex circularity ($\langle \mathcal{E}_0^2 \rangle = 0$), this yields $\langle |\mathcal{F}_\alpha|^4 \rangle = 2\langle |\mathcal{F}_\alpha|^2 \rangle^2 + |\langle \mathcal{F}_\alpha^2 \rangle|^2 = 2\langle |\mathcal{F}_\alpha|^2 \rangle^2$, leading to the familiar result $\sigma_{|F_\alpha|^2} = \langle |F_\alpha|^2 \rangle$ for $\alpha = x, y, z$ [10]. For the energies, this results in explicit functions of kz as

$$\sigma_{U_\alpha}(kz) = \left(1 \mp j_0 \pm \frac{j_2}{2}\right) \sigma_{U_{\alpha,\infty}}, \quad \alpha = x, y \quad (29)$$

$$\sigma_{U_z}(kz) = (1 \pm j_0 \pm j_2) \sigma_{U_{\alpha,\infty}} \quad (30)$$

in which upper and lower signs refer to electric ($U = U_e$, $\mathcal{F}_0 = \mathcal{E}_0$, $\varphi_0 = \epsilon_0$) and magnetic ($U = U_m$, $\mathcal{F}_0 = \mathcal{H}_0 = \mathcal{E}_0/\eta_0$, $\varphi_0 = \mu_0$) energy densities, respectively, and with

$$\sigma_{U_{\alpha,\infty}} = \langle U_{\alpha,\infty} \rangle = \frac{\varphi_0 \langle |\mathcal{F}_0|^2 \rangle}{3}, \quad \alpha = x, y, z. \quad (31)$$

For the energy density of the 2-D tangential electric or magnetic field, it follows from (29) and $U_t = U_x + U_y$ that

$$\sigma_{U_t}(kz) = \left(1 \mp j_0 \pm \frac{j_2}{2}\right) \sigma_{U_{t,\infty}} \quad (32)$$

where

$$\sigma_{U_{t,\infty}} = \frac{\sqrt{2} \varphi_0 \langle |\mathcal{F}_0|^2 \rangle}{3}. \quad (33)$$

For the full (vectorial) electric or magnetic energy density, the standard deviation follows from (29) and (30) as

$$\sigma_U(kz) = \sigma_{U_\infty} \sqrt{1 \mp \frac{2j_0}{3} \pm \frac{4j_2}{3} + j_0^2 + \frac{j_2^2}{2}} \quad (34)$$

where upper and lower signs again refer to electric and magnetic densities, respectively, and with

$$\sigma_{U_\infty} = \frac{\varphi_0 \langle |\mathcal{F}_0|^2 \rangle}{\sqrt{3}}. \quad (35)$$

These standard deviations are plotted in Fig. 2, comparing favourably with results in Figs. 6(b) and 7(b) of [10].²

For the combined EM energy density $U_{em(\alpha)} \equiv U_{e(\alpha)} + U_{m(\alpha)}$, the variances of its Cartesian tangential/normal, planar tangential, and full vectorial densities are found as

$$\sigma_{U_{em,\alpha}}^2 = \sigma_{U_{e,\alpha}}^2 + \sigma_{U_{m,\alpha}}^2, \quad \alpha = x, y, z \quad (36)$$

$$\sigma_{U_{em(t)}}^2 = \sigma_{U_{e(t)}}^2 + \sigma_{U_{m(t)}}^2 + |\langle E_x H_y^* \rangle|^2 / (2c)^2. \quad (37)$$

Explicit expressions for their standard deviations follow as

$$\sigma_{U_{em,\alpha}}(kz) = \sigma_{U_{em,\alpha,\infty}} \sqrt{1 + j_0^2 + \frac{j_2^2}{4} - j_0 j_2}, \quad \alpha = x, y \quad (38)$$

$$\sigma_{U_{em,z}}(kz) = \sigma_{U_{em,z,\infty}} \sqrt{1 + j_0^2 + j_2^2 + 2j_0 j_2} \quad (39)$$

$$\sigma_{U_{em,t}}(kz) = \sigma_{U_{em,t,\infty}} \sqrt{1 + j_0^2 + \frac{9j_1^2}{4} + \frac{j_2^2}{4} - j_0 j_2} \quad (40)$$

$$\sigma_{U_{em}}(kz) = \sigma_{U_{em,\infty}} \sqrt{1 + j_0^2 + \frac{3j_1^2}{2} + \frac{j_2^2}{2}} \quad (41)$$

²Note that in [10], energy densities were denoted by the symbol S .

where $\sigma_{U_{em(\alpha)(t)\infty}} = \sqrt{2} \sigma_{U_{(\alpha)(t)\infty}}$, i.e.,

$$\sigma_{U_{em,\alpha,\infty}} = \frac{\sqrt{2} \varphi_0 \langle |\mathcal{F}_0|^2 \rangle}{3}, \quad \alpha = x, y, z \quad (42)$$

$$\sigma_{U_{em,t,\infty}} = \frac{2 \varphi_0 \langle |\mathcal{F}_0|^2 \rangle}{3} \quad (43)$$

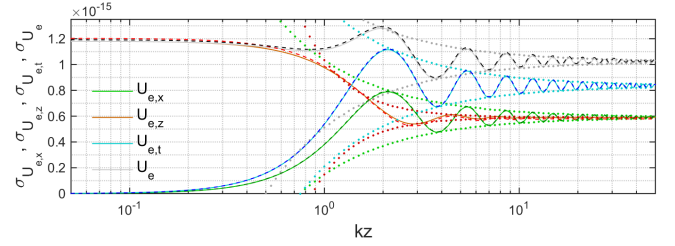
$$\sigma_{U_{em,\infty}} = \sqrt{\frac{2}{3}} \varphi_0 \langle |\mathcal{F}_0|^2 \rangle. \quad (44)$$

In (29), (30), (32) and (34), the terms linear in j_0 and j_2 cancel in their contributions to (38)–(41), leaving only quadratic terms. As shown in sec. V, this compensation between $U_{e(\alpha)}$ and $U_{m(\alpha)}$ produces faster (higher-order) power-law decays with kz in the envelopes of their sums $U_{em(\alpha)}$.

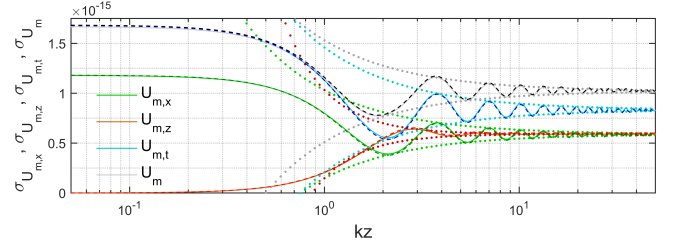
In summary, a PEC boundary induces different RMS levels of fluctuation for the Poynting vs. scalar power, i.e.,

$$\sigma_{S(\alpha)}(kz) \neq \sigma_{cU_{em(\alpha)}}(kz), \quad \alpha = x, y, z, t \quad (45)$$

complementing the result $j \langle S(\alpha)(kz) \rangle \neq \langle cU_{em(\alpha)}(kz) \rangle$ [1]. Fig. 1(b) shows (38)–(44), after scaling by c .



(a)



(b)

Fig. 2: Standard deviations, in units J/m^3 , based on $\langle \mathcal{E}_0'^2 \rangle^{1/2} = \langle \mathcal{E}_0''^2 \rangle^{1/2} = 0.01$ V/m, for (a) $U_{e,x}$, $U_{e,z}$, $U_{e,t}$, U_e , and (b) $U_{m,x}$, $U_{m,z}$, $U_{m,t}$, U_m . Solid: theory; dashed: MC simulation; dotted: asymptotic upper and lower envelopes. Olive/green: $U_{(e),(m),x}$; maroon/red: $U_{(e),(m),z}$; blue/cyan: $U_{(e),(m),t}$; black/gray: $U_{(e)(m)}$.

In applications to immunity, susceptibility or fading testing, the PEC boundary thus induces a kz -dependent scaling of the probability density functions (PDFs). For example, for the Cartesian field strength $|E_\alpha|$ with variance $\sigma_{|E_\alpha|}^2(kz) = [(4 - \pi)/\epsilon_0] \sigma_{U_{e,\alpha}}(kz)$ for $\alpha = x, y, z$, the scaling of its PDF

$$f_{|E_\alpha|}(|e_\alpha|, kz) = \frac{\epsilon_0 |e_\alpha|}{2\sigma_{U_{e,\alpha}}(kz)} \exp \left[-\frac{\epsilon_0 |e_\alpha|^2}{4\sigma_{U_{e,\alpha}}(kz)} \right] \quad (46)$$

is damped oscillatory, as governed by (29) or (30). In turn, this scaling affects associated statistics and distributions, e.g.,

$F_{|E_\alpha|_{\max}}(|e_\alpha|_{\max}, kz) = [F_{|E_\alpha|}(|e_\alpha|_{\max}, kz)]^{N(kz)}$ for the maximum field strength $|E_\alpha|_{\max}$. Fig. 3 demonstrates this scaling and bifurcation of (46) for actual (i.e., dimensioned, non-normalized) $|E_x|$ vs. $|E_z|$, at selected values of kz .

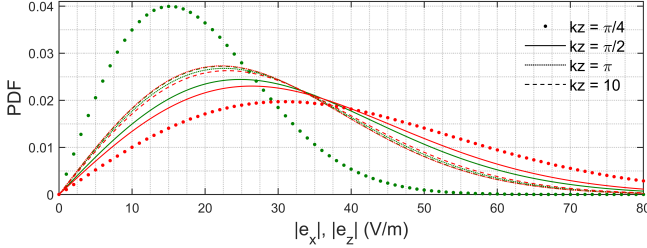


Fig. 3: Rayleigh PDFs (46) of $|E_x|$ (green) and $|E_z|$ (red) for $\langle \mathcal{E}_0'^2 \rangle^{1/2} = \langle \mathcal{E}_0''^2 \rangle^{1/2} = 20$ V/m, exhibiting kz -dependent scaling.

V. ASYMPTOTIC ENVELOPES AND RANGE OF σ

In [1, sec. III-C], asymptotic approximations by envelopes for the mean power and energy densities at $kz \gg 3/2$ were derived, resulting in simpler inverse power law expressions for their damped oscillations. Such nonlocal approximations are also useful when phase shifts arise that are caused by perturbations, e.g., apertures, scatterers, other nearby walls, boundary roughness, antenna-surface coupling, etc. Here, results for these envelopes of the mean are extended to corresponding envelopes for the standard deviation.

A. Linear Forms for Electric or Magnetic Energy Fluctuations

In (29), (30) and (32), the standard deviations have the form

$$\sigma_{U_\alpha}(kz) = (1 + a_0 j_0 + a_2 j_2) \sigma_{U_{\alpha,\infty}}. \quad (47)$$

Their associated asymptotic envelopes $\Upsilon_{U_\alpha}^\pm(kz \gg 3/2)$ can be obtained as the modulus of the corresponding analytic signal, $|\tilde{\sigma}_{U_\alpha}(kz \gg 3/2)|$. To this end, $\tilde{j}_\ell \triangleq j_\ell + j\mathbb{H}[j_\ell]$ for the individual terms in (47) are sought for $kz \gg 3/2$, where $\mathbb{H}[\cdot]$ denotes the Hilbert transform. Recall the asymptotic approximations

$$j_\ell \simeq \frac{\sin(2kz - \ell\pi/2)}{2kz} \quad \text{for } kz \gg \frac{\ell(\ell+1)}{4} \quad (48)$$

which, for even $\ell \equiv 2m$, result in

$$\mathbb{H}[j_{2m}(2kz \gg (2m+1)m)] \simeq (-1)^m \frac{1 - \cos(2kz)}{2kz}. \quad (49)$$

On the other hand, $z^{-1} \sin(2kz - \ell\pi/2)$ in (48) represents an amplitude modulated signal when $z \gg (2k)^{-1}$, for an arbitrary wavenumber $k > 0$. Therefore, on application of Bedrosian's theorem [14], it follows that

$$\tilde{j}_\ell = j_\ell + j\mathbb{H}[j_\ell] \simeq \frac{\exp[j(2kz - (\ell+1)\pi/2)]}{2kz} \quad (50)$$

whence $|\tilde{j}_\ell(2kz \gg 1)| \simeq (2kz)^{-1}$. Combining with $\mathbb{H}[1] = 0$ and applying the linearity of the Hilbert transform, upper ('+') and lower ('-') envelopes of $\sigma_{U_\alpha}(kz \gg 3/2)$ follow as

$$\Upsilon_{U_\alpha}^\pm(kz \gg 3/2) \simeq \begin{cases} \left[1 \pm \frac{|a_0 - a_2|}{2(kz)}\right] \sigma_{U_{\alpha,\infty}}, & a_0 - a_2 \neq 0, \\ \left[1 \pm \frac{3|a_2|}{4(kz)^2}\right] \sigma_{U_{\alpha,\infty}}, & a_0 - a_2 = 0. \end{cases} \quad (51)$$

Thus, the envelopes decay typically³ according to a first-order power law, $(kz)^{-1}$. Application of (51) to (29), (30) and (32) yields the asymptotic envelopes of $\sigma_{U_{(\alpha)(t)}}(kz \gg 3/2)$ as

$$\Upsilon_{U_\alpha}^\pm(kz \gg 3/2) \simeq \left[1 \pm \frac{3}{4kz}\right] \sigma_{U_{\alpha,\infty}}, \quad \alpha = x, y \quad (52)$$

$$\Upsilon_{U_z}^\pm(kz \gg 3/2) \simeq \left[1 \pm \frac{3}{4(kz)^2}\right] \sigma_{U_{z,\infty}} \quad (53)$$

$$\Upsilon_{U_t}^\pm(kz \gg 3/2) \simeq \left[1 \pm \frac{3}{4kz}\right] \sigma_{U_{t,\infty}}. \quad (54)$$

By contrast, close to the PEC boundary, using

$$j_\ell \simeq \frac{(2kz)^\ell}{(2\ell+1)!!} \left[1 - \frac{(2kz)^2}{2(2\ell+3)}\right] \quad \text{for } kz \ll \sqrt{2\ell+5} \quad (55)$$

all $\sigma_{U_{(\alpha)(t)}}(kz)$ are quadratic in kz to leading order, viz.,

$$\sigma_{U_{e(\alpha)(t)}}(kz \ll \sqrt{5}) \simeq \frac{4(kz)^2}{5} \sigma_{U_{e(\alpha)(t),\infty}}, \quad \alpha = x, y \quad (56)$$

$$\sigma_{U_{e,z}}(kz \ll \sqrt{5}) \simeq 2 \left[1 - \frac{(kz)^2}{5}\right] \sigma_{U_{e,z,\infty}} \quad (57)$$

$$\sigma_{U_{m(\alpha)(t)}}(kz \ll \sqrt{5}) \simeq 2 \left[1 - \frac{2(kz)^2}{15}\right] \sigma_{U_{m(\alpha)(t),\infty}} \quad (58)$$

$$\sigma_{U_{m,z}}(kz \ll \sqrt{5}) \simeq \frac{2(kz)^2}{5} \sigma_{U_{m,z,\infty}}. \quad (59)$$

B. Quadratic Forms for EM Energy or Power Fluctuations

In (17), (22), (24) and (27), the variances have the form

$$\sigma_{S_{(\alpha)}}^2(kz) = (1 + a_{00}j_0^2 + a_{22}j_2^2 + a_{02}j_0j_2) \sigma_{S_{(\alpha),\infty}}^2. \quad (60)$$

For their asymptotic envelopes, a derivation analogous to that in sec. V-A can be performed. With

$$j_{2m}^2 \simeq \frac{2[1 - \cos(4kz)]}{(4kz)^2}, \quad \mathbb{H}[j_{2m}^2] \simeq \frac{2[4kz - \sin(4kz)]}{(4kz)^2} \\ j_{2m}j_{2m+2} \simeq \frac{2\sin(4kz)}{(4kz)^2}, \quad \mathbb{H}[j_{2m}j_{2m+2}] \simeq -\mathbb{H}[j_{2m}^2] \quad (61)$$

for $kz \gg 3/2$, envelopes for $\sigma_{S_{(\alpha)}}^2(kz)$ can then be converted to envelopes $\Upsilon_{S_{(\alpha)}}^\pm(kz)$ for $\sigma_{S_{(\alpha)}}(kz)$, on expanding $\sigma_{S_{(\alpha)}}(kz)$ in (60) using $\sqrt{1+x} \simeq 1 + x/2$ for $x \ll 1$. This results in⁴

$$\Upsilon_{S_{(\alpha)}}^\pm(kz \gg 3/2) \simeq \sigma_{S_{(\alpha),\infty}} \times \begin{cases} \left[1 \pm \frac{|a_{00} + a_{22} - a_{02}|}{8(kz)^2}\right], & a_{00} + a_{22} - a_{02} \neq 0, \\ \left[1 \pm \frac{3|2a_{22} - a_{02}|}{32(kz)^3}\right], & a_{00} + a_{22} - a_{02} = 0. \end{cases} \quad (62)$$

³If $a_0 - a_2 = 0$, e.g., for U_z , the envelopes are found by first replacing j_2 by its exact expression $[3/(2kz)]j_1 - j_0$ instead of the approximation $-j_0$.

⁴A similar remark as in sec. V-A for U_z holds if $a_{00} + a_{22} - a_{02} = 0$.

The fluctuations of the tangential power are decaying at a faster (cubic) rate than the quadratic rate of the normal and full vector Poynting powers, viz.,

$$\Upsilon_{S_{(\alpha)(t)}}^{\pm}(kz \gg 3/2) \simeq \left[1 \pm \frac{9}{64(kz)^3}\right] \sigma_{S_{(\alpha)(t),\infty}}, \quad \alpha = x, y \quad (63)$$

$$\Upsilon_{S_z}^+ = \sigma_{S_z,\infty}, \quad \Upsilon_{S_z}^-(kz \gg 3/2) \simeq \left[1 - \frac{9}{32(kz)^2}\right] \sigma_{S_z,\infty} \quad (64)$$

$$\Upsilon_S^{\pm}(kz \gg 3/2) \simeq \left[1 \pm \frac{3}{32(kz)^2}\right] \sigma_{S,\infty}. \quad (65)$$

Unlike $\Upsilon_{U_{(\alpha)}}^{\pm}(kz)$, which exhibit the same kz -dependence as the envelopes $\Xi_{U_{(\alpha)}}^{\pm}(kz)$ for $\langle U_{(\alpha)}(kz) \rangle$ [1, eqs. (34)–(36)], the $\Upsilon_{S_z}^{\pm}(kz)$ decay more rapidly than $\Xi_{S_z}^{\pm}(kz)$ [1, eq. (33)]. Near the boundary, $\sigma_{S_z}(kz)$ exhibits a *linear* dependence, all other Poynting powers being quadratic in kz , i.e.,

$$\sigma_{S_{(\alpha)(t)}}(kz \ll \sqrt{5}) \simeq \sqrt{2} \left[1 - \frac{3(kz)^2}{10}\right] \sigma_{S_{(\alpha)(t),\infty}, \quad \alpha = x, y \quad (66)$$

$$\sigma_{S_z}(kz \ll \sqrt{5}) \simeq \sqrt{\frac{8}{5}} kz \sigma_{S_z,\infty} \quad (67)$$

$$\sigma_S(kz \ll \sqrt{5}) \simeq \frac{2}{\sqrt{3}} \left[1 - \frac{(kz)^2}{10}\right] \sigma_{S,\infty}. \quad (68)$$

For the total EM energy densities (38)–(41), the upper envelopes $\Upsilon_{U_{em(\alpha)(t)}}^+(kz)$ follow in a similar way as

$$\Upsilon_{U_{em,\alpha}}^+(kz \gg 3/2) \simeq \left[1 + \frac{9}{32(kz)^2}\right] \sigma_{U_{em,\alpha,\infty}}, \quad \alpha = x, y \quad (69)$$

$$\Upsilon_{U_{em,z}}^+(kz \gg 3/2) \simeq \left[1 + \frac{9}{32(kz)^4}\right] \sigma_{U_{em,z,\infty}} \quad (70)$$

$$\Upsilon_{U_{em,t}}^+(kz \gg 3/2) \simeq \left[1 + \frac{9}{32(kz)^2}\right] \sigma_{U_{em,t,\infty}} \quad (71)$$

$$\Upsilon_{U_{em}}^+(kz \gg 3/2) \simeq \left[1 + \frac{3}{16(kz)^2}\right] \sigma_{U_{em,\infty}}. \quad (72)$$

In particular, $\Upsilon_S^+(kz \gg 3/2)$ and $\Upsilon_{cU_{em}}^+(kz \gg 3/2)$ decay at identical quadratic rates and magnitudes. The $\Upsilon_{U_{em,\alpha}}^-(kz \gg 3/2)$ coincide with $\sigma_{U_{em,\alpha,\infty}}$, whereas $\Upsilon_{U_{em,t}}^-(kz \gg 3/2)$ and $\Upsilon_{U_{em}}^-(kz \gg 3/2)$ exhibit no significant oscillations, whence

$$\Upsilon_{U_{em,\alpha}}^-(kz \gg 3/2) \simeq \sigma_{U_{em,\alpha,\infty}}, \quad \alpha = x, y, z \quad (73)$$

$$\Upsilon_{U_{em}(t)}^-(kz \gg 3/2) \simeq \Upsilon_{U_{em}(t)}^+(kz \gg 3/2). \quad (74)$$

Near the boundary, $\sigma_{cU_{em(x)(t)}}(kz) \simeq \sigma_{S(x)(t)}(kz)$ while $\sigma_{cU_{em(z)}}(kz) > \sigma_{S_z}(kz)$, as seen in Fig. 1. Explicitly,

$$\sigma_{U_{em,\alpha}}(kz \ll \sqrt{5}) \simeq \sqrt{2} \left[1 - \frac{2(kz)^2}{5}\right] \sigma_{U_{em,\alpha,\infty}}, \quad \alpha = x, y \quad (75)$$

$$\sigma_{U_{em,z}}(kz \ll \sqrt{5}) \simeq \sqrt{2} \left[1 - \frac{(kz)^2}{5}\right] \sigma_{U_{em,z,\infty}} \quad (76)$$

$$\sigma_{U_{em,t}}(kz \ll \sqrt{5}) \simeq \sqrt{2} \left[1 - \frac{3(kz)^2}{10}\right] \sigma_{U_{em,t,\infty}} \quad (77)$$

$$\sigma_{U_{em}}(kz \ll \sqrt{5}) \simeq \sqrt{2} \left[1 - \frac{(kz)^2}{2}\right] \sigma_{U_{em,\infty}}. \quad (78)$$

C. Mixed Linear-Quadratic Forms for 3-D Vectorial Electric or Magnetic Energy Fluctuations

If $\sigma(kz)$ contains both linear and quadratic terms in j_ℓ , e.g., for U in (34), then the weaker decay for the linear terms – typically a $(kz)^{-1}$ -law – prevails for $kz \gg 3/2$. Thus,

$$\Upsilon_U^{\pm}(kz \gg 3/2) \simeq \left[1 \pm \frac{1}{2kz}\right] \sigma_{U,\infty} \quad (79)$$

for $U = U_e$ or U_m . Near the boundary,

$$\sigma_{U_e}(kz \ll \sqrt{5}) \simeq \frac{2}{\sqrt{3}} \left[1 - \frac{2(kz)^2}{15}\right] \sigma_{U_e,\infty} \quad (80)$$

$$\sigma_{U_m}(kz \ll \sqrt{5}) \simeq \sqrt{\frac{8}{3}} \left[1 - \frac{2(kz)^2}{3}\right] \sigma_{U_m,\infty}. \quad (81)$$

VI. RELATIVE LEVELS OF FLUCTUATION

A. Coefficient of Variation

The coefficient of variation (CV), $\nu_X \triangleq \sigma_X/\langle X \rangle$, represents the mean-normalized RMS level of fluctuation of X , as a simple measure of its relative uncertainty. Its reciprocal, $1/\nu_X$, measures the SNR of X . Close to the boundary, the CV differs considerably between the various components of the powers S or cU_{em} . On the boundary itself,

$$\nu_{S_z}(0) = j2/\sqrt{5}, \quad \nu_S(0) = \lim_{kz \rightarrow 0^+} j\sqrt{2}/(kz) = +j\infty \quad (82)$$

$$\nu_{cU_{em,\alpha}}(0) = \sqrt{2}\nu_{cU_{em,t}}(0) = \sqrt{3}\nu_{cU_{em}}(0) = 1. \quad (83)$$

Fig. 4(a) shows the SNRs $j/\nu_{S_z}(kz)$ and $j/\nu_S(kz)$, confirming that $|\nu_S(kz)| \geq |\nu_{S_z}(kz)|$ for arbitrary kz and that both CVs are in phase for $kz \gg 3/2$. Fig. 4(b) shows selected CVs $\nu_{U_{em(\alpha)}}(kz) \equiv \nu_{cU_{em(\alpha)}}(kz)$. Comparing with Fig. 4(a), a slightly smaller relative uncertainty of S_z over $U_{e,z}$ (up to 11.8%, on the boundary) is achieved for $kz < 1$, while for $kz > 1$ the relative uncertainty for S_z is much larger. The constancy of $\nu_{U_{e,z}}(kz)$ and $\nu_{U_{m,t}}(kz)$ indicates that the χ_2^2 and χ_4^2 PDFs of the respective deep energies are maintained at any distance, up to the boundary. The variation of $\nu_{U_e}(kz)$ from 1 at $kz = 0$ to $1/\sqrt{3}$ at $kz \rightarrow +\infty$ is a testimony of the compound exponential PDF [15] for the full $U_e(kz)$, evolving from χ_2^2 to χ_6^2 . The $U_{em}(kz)$ has a corresponding evolution, from χ_6^2 for $U_{em}(0) = U_{e,z}(0) + U_{m,t}(0)$ with $\nu_{U_{em}}(0) = 1/\sqrt{3}$, to χ_{12}^2 for $U_e(kz \rightarrow \infty) + U_m(kz \rightarrow \infty)$ and $\nu_{U_{em}}(\infty) = 1/\sqrt{6}$. All $\nu_{cU_{em(\alpha)}}(kz)$ are rescalings of the $\sigma_{cU_{em(\alpha)}}(kz) \equiv c\sigma_{U_{em(\alpha)}}(kz)$ shown in Fig. 1(b), because all $\langle U_{em(\alpha)} \rangle$ are independent of kz . Fig. 4 also indicates that

$$\nu_{cU_{em}}(kz) \ll |\nu_S(kz)| \quad (84)$$

at any kz , differing typically by an order of magnitude or more. As a practical consequence, the conversion of the intensity or energy measured using electric and magnetic field probes to the scalar EM power produces considerably lower relative uncertainty than the direct measurement of Poynting power using aperture antennas, at any distance from the boundary.

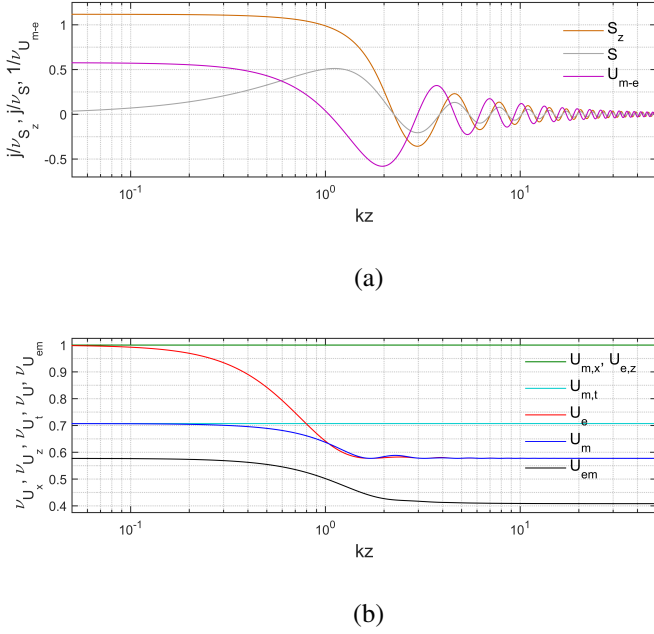


Fig. 4: Relative fluctuations as a function of kz : (a) SNRs j/ν_{S_z} (brown), j/ν_S (gray), and $1/\nu_{U_{m-e}}$ (purple); (b) CVs $\nu_{U_{m,x}}$ (green), $\nu_{U_{e,z}}$ (green), $\nu_{U_{m,t}}$ (cyan), ν_{U_e} (red), ν_{U_m} (blue), and $\nu_{U_{em}}$ (black).

B. Coefficient of Range Variation

The CV measures the actual standard deviation relative to the actual mean value, both at the same location. Related to their respective envelopes, the *coefficient of range variation* (CRV) of X , denoted as ζ_X , is here introduced as the ratio of the local range of variation between $\Upsilon_X^+(kz)$ and $\Upsilon_X^-(kz)$ for σ_X at kz to the corresponding range of $\Xi_X^\pm(kz)$ for the real or complex $\langle X \rangle$ at the same kz , i.e.,

$$\zeta_X(kz) \triangleq \frac{\Upsilon_X^+(kz) - \Upsilon_X^-(kz)}{\Xi_X^+(kz) - \Xi_X^-(kz)}. \quad (85)$$

This measure is particularly useful when nonlocal deviations are expected from ideal $\sigma_X(kz)$ or $\langle X(kz) \rangle$ and hence $\nu_X(kz)$, e.g., for causes of field perturbations listed in sec. V. For $kz \gg 3/2$, the CRVs for the Poynting power components are

$$\zeta_{S_\alpha}(kz \gg 3/2) = \frac{9\sigma_{S_{\alpha,\infty}}/[32(kz)^3]}{\langle S_{\alpha,\infty} \rangle} \rightarrow \infty, \quad \alpha = x, y \quad (86)$$

$$\zeta_{S_z}(kz \gg 3/2) = \frac{9\sigma_{S_{z,\infty}}/[32(kz)^2]}{-j\langle |\mathcal{E}_0|^2/\eta_0 \rangle/(kz)} = j\frac{3\sqrt{2}}{32kz} \quad (87)$$

$$\zeta_{S_t}(kz \gg 3/2) = \frac{9\sigma_{S_{t,\infty}}/[32(kz)^3]}{\langle S_{t,\infty} \rangle} \rightarrow \infty \quad (88)$$

$$\zeta_S(kz \gg 3/2) = \frac{3\sigma_{S_\infty}/[16(kz)^2]}{-j\langle |\mathcal{E}_0|^2/\eta_0 \rangle/(kz)} = j\frac{\sqrt{6}}{16kz}. \quad (89)$$

The decrease of $\zeta_{S_{(z)}}(kz)$ according to $(kz)^{-1}$ signifies that the nonlocal range of σ_{S_z} decays more rapidly with kz than that of $\langle S_z \rangle$ for $kz \gg 3/2$. At these large distances, it follows that $|\zeta_{S_{(z)}}(kz \gg 3/2)| \ll 1$.

Similarly, for the electric or magnetic energy densities

$$\zeta_{U_\alpha}(kz \gg 3/2) = \frac{3\sigma_{U_{\alpha,\infty}}/(2kz)}{3\langle U_{\alpha,\infty} \rangle/(2kz)} = 1, \quad \alpha = x, y \quad (90)$$

$$\zeta_{U_z}(kz \gg 3/2) = \frac{3\sigma_{U_{z,\infty}}/[2(kz)^2]}{3\langle U_{z,\infty} \rangle/[2(kz)^2]} = 1 \quad (91)$$

$$\zeta_{U_t}(kz \gg 3/2) = \frac{3\sigma_{U_{t,\infty}}/(2kz)}{3\langle U_{t,\infty} \rangle/(2kz)} = \frac{1}{\sqrt{2}} \quad (92)$$

$$\zeta_U(kz \gg 3/2) = \frac{\sigma_{U_\infty}/(kz)}{\langle U_\infty \rangle/(kz)} = \frac{1}{\sqrt{3}}. \quad (93)$$

Unlike $\zeta_{S_{(\alpha)}}$, all $\zeta_{U_{(\alpha)}}$ are finite and independent of kz . Note that $\zeta_{U_{(\alpha)}}(kz \gg 3/2) = \nu_{U_{(\alpha),\infty}}$ even though all $\sigma_{U_{(\alpha)}}(kz)$ exhibit oscillations, as seen in Fig. 2. All $\zeta_{U_{em,(\alpha)}}(kz)$ are infinite because all $\langle U_{em,(\alpha)}(kz) \rangle$ are independent of kz .

VII. POYNTING'S THEOREM FOR RMS FLUCTUATIONS

Poynting's theorem of energy conservation links the local power flux for deterministic fields to the energy imbalance as

$$\nabla \cdot \underline{S}(\underline{r}) = -j\omega[U_m(\underline{r}) - U_e(\underline{r})] \triangleq -j\omega U_{m-e}(\underline{r}). \quad (94)$$

For deterministic or random plane waves ($\nabla = -jk\hat{k}$) with fixed \hat{k} , (94) reduces to $S_k(\underline{r}) = cU_m(\underline{r}) - cU_e(\underline{r})$, expressing the \hat{k} -directed Poynting component $S_k \equiv \underline{S} \cdot \hat{k}$ as the imbalance between the magnetic and electric scalar power densities. For stochastic fields, it was shown in [1] that (94) also holds for the mean power and energy densities, i.e.,

$$\langle \nabla \cdot \underline{S}(kz) \rangle = \nabla \cdot \langle \underline{S}(kz) \rangle = -j\omega \langle U_{m-e}(kz) \rangle. \quad (95)$$

Complex conjugation of (94) followed by side-by-side multiplication and ensemble averaging for random fields shows that the second-order moments are correspondingly related as

$$\langle |\nabla \cdot \underline{S}(kz)|^2 \rangle = \omega^2 \langle |U_{m-e}(kz)|^2 \rangle. \quad (96)$$

With $\sigma_{U_{m-e}} = \sigma_{U_{em}}$ and (44), Poynting's theorem for RMS fluctuations at any kz follows from (95) and (96) as

$$\sigma_{\nabla \cdot \underline{S}}(kz) = \omega \sigma_{U_{m-e}}(kz) = \omega \sigma_{U_{em,\infty}} \sqrt{1 + j_0^2 + \frac{3j_1^2}{2} + \frac{j_2^2}{2}}. \quad (97)$$

The average energy imbalance for arbitrary kz [1, eq. (47)]

$$\langle U_{m-e}(kz) \rangle = \frac{2\varphi_0 \langle |\mathcal{F}_0|^2 \rangle}{3} (j_0 - 2j_2) \quad (98)$$

is plotted in [1, Fig. 5]. Near the boundary,

$$\langle U_{m-e}(kz \ll \sqrt{5}) \rangle \simeq \frac{2\varphi_0 \langle |\mathcal{F}_0|^2 \rangle}{3} \left[1 - \frac{6(kz)^2}{5} \right] \quad (99)$$

i.e., quadratically approaching $\langle U_{m,x}(0) \rangle = \langle U_{e,z}(0) \rangle = \langle U_{em,t}(0) \rangle = \langle U_{em}(0) \rangle/3$ for $kz \rightarrow 0$. Its asymptotic envelopes are

$$\Xi_{U_{m-e}}^\pm(kz \gg 3/2) \simeq \pm \frac{\varphi_0 \langle |\mathcal{F}_0|^2 \rangle}{kz}. \quad (100)$$

The CV of U_{m-e} (or cU_{m-e}) at arbitrary distances is

$$\nu_{U_{m-e}}(kz) = \sqrt{\frac{3(1 + j_0^2 + \frac{3}{2}j_1^2 + \frac{1}{2}j_2^2)}{8(j_0 - 2j_2)^2}}. \quad (101)$$

Its reciprocal is plotted in Fig. 4(a). From its range of values across kz , it can be inferred that, even though Poynting's law holds equally between the average power flux and the average energy imbalance as well as between their respective RMS fluctuation levels, the exchanges between the fluctuations are stronger, i.e., $\sigma_{U_{m-e}}(kz) \gg \langle U_{m-e}(kz) \rangle$ for general kz . This is *a fortiori* the case for $kz \gg 1$, where $\langle \underline{S} \rangle$ and hence $\nabla \cdot \langle \underline{S} \rangle$ approach null. Consequently, $\nu_{U_{m-e}}(kz)$ approaches infinity for $kz \rightarrow +\infty$, also at quasi-periodic finite distances.

On the boundary, $\nu_{U_{m-e}}$ reaches its minimum value $\sqrt{3}$ that exceeds 1, i.e., the RMS fluctuation of the EM energy imbalance always remains larger than the mean imbalance, further increasing quadratically with distance as

$$\nu_{U_{m-e}}(kz \ll \sqrt{5}) \simeq \sqrt{3} \left[1 + \frac{7(kz)^2}{10} \right]. \quad (102)$$

From (72), (74) and (100), the CRV $\zeta_{U_{m-e}}(kz \gg 3/2)$ varies as $(kz)^{-1}$ and coincides with $|\zeta_S(kz \gg 3/2)|$, i.e.,

$$\begin{aligned} \zeta_{U_{m-e}}(kz \gg 3/2) &= \frac{3\sigma_{U_{em,\infty}}/[8(kz)^2]}{2\varphi_0\langle |\mathcal{F}_0|^2 \rangle / (kz)} \\ &= \frac{\sqrt{6}}{16kz} = |\zeta_S(kz \gg 3/2)|. \end{aligned} \quad (103)$$

VIII. CONCLUSION

In this article, the scalar EM power density cU_{em} as a converted and scaled EM energy density and the Poynting vector \underline{S} for harmonic random fields were analyzed. The divergence of \underline{S} is proportional to $U_m - U_e$, whereas cU_{em} is proportional to $U_m + U_e$. For deterministic plane waves ($\underline{E} = \eta_0 \underline{H} \times \underline{1}_k$, $\underline{k} \cdot \underline{E} = 0$), both power quantities yield the same value. In random non-plane wave environments, only the latter produces a nontrivial mean value in free space. The presence of an ideal PEC boundary affects both their means and standard deviations in different ways; cf. (4) vs. (8) and (27) vs. (41). For random fields near a PEC boundary, $U_e(kz) \neq U_m(kz)$ qualitatively and quantitatively. The results indicate the need for evaluating both \underline{E} and \underline{H} to obtain statistics of random EM power or energy density, unlike for deterministic plane waves where knowledge of either field suffices.

For Cartesian, tangential and full vectorial power and energy densities near a PEC boundary, their local standard deviations were obtained as eqs. (17), (22), (24), (27); eqs. (29), (30), (32), (34); and eqs. (38)–(41), respectively. Similar to the averages, these standard deviations exhibit power-law type decay with the electrical distance kz , on average, at different rates. For the EM power, the envelope of σ_{S_x} converges most rapidly to the free-space value, decaying as $(kz)^{-3}$. For the energy densities U_e and U_m , the most rapid decay as $(kz)^{-2}$ occurs for the normal components σ_{U_z} ; cf. (53). For 3-D vector fields, the standard deviation for power decays according to $(kz)^{-2}$ in (62), which is more rapidly than $(kz)^{-1}$ for energy in (79). Only the normal components σ_{S_z} and σ_{U_z} exhibit the same $(kz)^{-2}$ decay. Thus, the standard deviations exhibit an equal or sharper roll-off and narrower transition zone of kz than the corresponding averages. Near the boundary, σ_{S_z}

increases linearly with kz , while all other standard deviations vary quadratically, to leading order.

On approaching the PEC boundary, for $kz \ll \sqrt{5}$, the absolute RMS fluctuations of the normal and full scalar vs. Poynting powers diverge, i.e., $\sigma_{cU_{em}(kz)} > \sigma_{S_z}$ (Fig. 1). As a consequence, this may affect criteria for acceptable levels of field nonuniformity in MSRC validation procedures [9], depending on whether dipole antennas or sensors vs. aperture antennas are used, when extending the working volume to include locations within the boundary zone. The relative RMS fluctuation of S is much larger than for cU_{em} , at any kz ; cf. (84). On the boundary, the CV of S_z is finite, unlike the CV of S ; cf. (82). For $kz \gg 3/2$, the decay of ζ_{S_z} occurs according to $(kz)^{-1}$ in (87), indicating that the range of nonlocal variation of $\sigma_{S_z}(kz)$ becomes progressively weaker with distance than that for $\langle S_z(kz) \rangle$. By contrast, the CRVs for energies in (90)–(93) are constant and coincide with their respective CVs.

The Poynting theorem, valid for averages of random power flux and random energy imbalance [1], extends to (97) for their standard deviations. The RMS fluctuations of the power flux and imbalance are larger than their mean values, as expressed by (101) and (102).

REFERENCES

- [1] L. R. Arnaut and G. Gradoni, "Average linear and angular momentum and power of random fields near a perfectly conducting boundary," *IEEE Trans. Electromagn. Compat.*, vol. 62, no. 4, pp. 1118–1127, Aug. 2020.
- [2] A. De Leo, G. Cerri, P. Russo, and V. Mariani Primiani, "A novel emission test method for multiple monopole source stirred reverberation chambers," *IEEE Trans. Electromagn. Compat.*, vol. 62, no. 5, pp. 2334–2337, Oct. 2020.
- [3] S. M. Smith and C. Furse, "Stochastic FDTD for analysis of statistical variation in electromagnetic fields," *IEEE Trans. Ant. Propag.*, vol. 60, no. 7, pp. 3343–3350, Jul. 2012.
- [4] D. A. Hill, *Electromagnetic Theory of Reverberation Chambers*. NIST Techn. Note 1506, U.S. Dep. Commerce, Boulder, CO, Dec. 1998.
- [5] J. M. Dunn, "Local, high-frequency analysis of the field in a mode-stirred chamber," *IEEE Trans. Electromagn. Compat.*, vol. 32, no. 1, pp. 53–58, Feb. 1990.
- [6] D. A. Hill, "Boundary fields in reverberation chamber," *IEEE Trans. Electromagn. Compat.*, vol. 47, no. 2, pp. 281–290, May 2005.
- [7] L. R. Arnaut, "Spatial correlation functions of inhomogeneous random electromagnetic fields," *Phys. Rev. E*, vol. 73, no. 3, 036604, Mar. 2006.
- [8] L. R. Arnaut, "Probability distribution of random electromagnetic fields in the presence of a semi-infinite isotropic medium," *Radio Sci.*, vol. 42, RS3001, 2007.
- [9] IEC Joint Task Force CISPR/A-SC77B: IEC 61000-4-21 Electromagnetic Compatibility (EMC) – Part 4-21: Testing and Measurement Techniques – Reverberation Chamber Test Methods, International Electrotechnical Commission, 2nd ed., Jan. 2011.
- [10] L. R. Arnaut and P. D. West, "Electromagnetic reverberation near a perfectly conducting boundary," *IEEE Trans. Electromagn. Compat.*, vol. 48, no. 2, pp. 359–371, May 2006.
- [11] L. R. Arnaut, "Measurement uncertainty in reverberation chambers: I. Sample statistics," *NPL Report TQE2*, 2nd ed., Nat. Phys. Lab., Teddington, U.K., Dec. 2008.
- [12] R. Serra and C. Carobbi, "A probabilistic interpretation of the IEC 61000-4-21 threshold levels for field uniformity in ideal reverberation chambers," *Proc. 2020 EMC Europe Int. Symp. Electromagn. Compat.*, 23–25 Sep. 2020, Rome, Italy.
- [13] A. M. Yaglom, *An Introduction to the Theory of Stationary Random Functions*. Prentice-Hall: Englewood Cliffs, N. J., 1962.
- [14] F. W. King, *Hilbert Transforms*. Cambridge University Press: Cambridge, U.K., 2009.
- [15] L. R. Arnaut, "Compound exponential distributions for undermoded reverberation chambers," *IEEE Trans. Electromagn. Compat.*, vol. 44, no. 3, pp. 442–457, Aug. 2002.